https://doi.org/10.5194/tc-2023-122
Preprint. Discussion started: 14 August 2023

The Cryosphere Discussions

The Variability of CryoSat-2 derived Sea Ice Thickness introduced by modelled vs. empirical snow thickness, sea ice density and water density

Imke Sievers[1,2], Henriette Skourup[3], and Till A. S. Rasmussen[1]

[1]Danish Meteorological Institut, Lyngbyvej 100, Copenhagen East, Denmark
[2]Aalborg University, A. C. Meyers Vænge 15, 2450 Copenhagen, Denmark
[3]DTU Space, Danish Technical University, Elektrovej Building 327, 2800 Kongens Lyngby, Denmark

Correspondence: Imke Sievers (imksie@dmi.dk)

Abstract. To derive sea ice thickness (SIT) from CryoSat-2 freeboard (FB) estimates, assumptions about snow thickness, snow density, sea ice density and water density need to be made. These parameters are close to impossible to observe alongside FB, so many existing products use climatologies, or empirical values. A resent study proposed to use model parameters for snow thickness, sea ice density and water density instead. In this study, we are evaluating this values against in situ observations and the commonly used climatologies and empirical values. We show that the snow thickness and water density is in better agreement with observations, and that the sea ice density is overall too light. Analyzing the difference in SIT resulting from the model parameter vs. the empirical values, we find that the snow thickness leads to the largest differences with up to 30 cm, closely followed by the sea ice density with 20 cm. For the water density we find an up to 7.5 cm difference, which is small in comparison to the snow thickness and sea ice density, but not negligible as most studies currently argue. We find that the origin of the assumption that water density is negligible in the FB to SIT conversion originates from a study investing the seasonal Arctic sea ice density variability, not taking into account the spacial variability. For CryoSat-2 based SIT products we recommend to either use a water density climatology, or an uncertainty value of 2.5 kgm^{-3} instead of the commonly used value of 0 to 0.5 kgm^{-3}.

1 Introduction

With help of radar or laser satellites, freeboard (FB) can be observed from space. From these observations, it is possible to derive Arctic wide sea ice thickness (SIT) estimates (Laxon et al., 2003; Tilling et al., 2018; Hendricks et al., 2021; Guerreiro and Fleury, 2017). The satellite with the longest time series of FB is Cryosat-2, which has observed the sea ice since 2010. Cryosat-2 was designed under the assumption that the radar signal gets reflected from the snow-ice interface and thereby measures the ice FB (Beaven et al., 1995; Wingham et al., 2006). Shortly after the launch, several studies found that the snow layer strongly influences the radar reflection horizon (Willatt et al., 2011; Kwok et al., 2011). To better describe what CryoSat-2 measures, Ricker et al. (2014) introduced the term radar FB. To derive SIT from the radar FB (FB_r), Archimedes principle is

https://doi.org/10.5194/tc-2023-122
Preprint. Discussion started: 14 August 2023

applied, and the SIT is derived as follows (Tilling et al., 2018):

$$SIT = \frac{(FB_r + 0.25 * H_s)\rho_w}{(\rho_w - \rho_i)} + \frac{H_s \rho_s}{(\rho_w - \rho_i)} \quad (1)$$

The terms in this equation are the snow thickness (H_s), the snow density (ρ_s), the ice density (ρ_i) and the water density (ρ_w). Alexandrov et al. (2010) conducted an error estimate study on equation 1 (excluding the radar FB correction term) and found that the largest contributors were the sea ice FB and the sea ice density. Another sensitivity study performed by (Kern et al., 2015) found that the snow thickness is at least as important as the sea ice density for the FB to SIT conversion. Prior to Alexandrov et al. (2010) the same sea ice density was used throughout the entire Arctic (Laxon et al., 2003). To address the sensitivity of equation 1 to sea ice density, (Alexandrov et al., 2010) introduced a method to derive the SIT depending on ice type, deriving sea ice density for multi year ice (MYI) and first year ice (FYI). This method, covering FB to SIT by using MYI and FYI values for the sea ice density in equation 1 (and in later versions also for snow thickness and snow density), will be called the classical approach in the following text. For snow density, snow thickness and water density they used values prior introduced by Laxon et al. (2003), where the Laxon et al. (2003) values for snow density and snow thickness originate from a snow thickness climatology by Warren et al. (1999) (W99). W99 is a snow thickness and density climatology compiled of 37 years of snow observations made at drift stations on the Arctic ice in the years 1954-91. Since it is a climatology, no interannual variability in snow thickness is included. Kurtz and Farrell (2011) found that due to changed sea ice conditions in the Arctic, W99 snow thicknesses should be reduced over FYI by 50%. Sallila et al. (2019) compared six different SIT products using Cryosat-2 FB to derive SIT and found that the majority of these products still use Alexandrov et al. (2010) values for sea ice density, the reduced W99 climatological values for snow density and thickness over FYI and a single value of varying magnitude for water density. Other sea ice products available since Sallila et al. (2019) use snow models as an alternative to the modified W99 (Fiedler et al., 2022; Landy et al., 2022), and some of the SIT products included in Sallila et al. (2019) have since started to use other snow thickness products over FYI, (Hendricks et al., 2021) i.e., from passive microwave. Apart from the changes in snow thickness, most of the values in equation 1 remain the same, as suggested by Alexandrov et al. (2010) and Laxon et al. (2003). The reason for using these values up until today is due to the fact that observations of the Arctic sea ice are sparse. A few studies have suggested different values for sea ice densities (Jutila et al., 2021; Ji et al., 2021). Ji et al. (2021) showed that the suggested sea ice density values from a climatology derived from observations from 2011-2015 improve SIT estimates in the Beaufort Sea compared to using the fixed values from Alexandrov et al. (2010). However, the observations used in this climatology are sparse with significantly more observations close to the validation site in the Beaufort Sea, which means that more validation is needed before relying on the derived sea ice densities in other regions. Jutila et al. (2021) uses airborne observations to derive bulk sea ice density and finds that sea ice in the Arctic has become denser over the past decades. They also derive a negative exponential relationship between the bulk density and the FB, but they acknowledge that more research is needed in order to use this relationship in FB to SIT retrievals. Sievers et al. (2023) used ice model sea ice density values to convert assimilated FB to SIT. They also used model values for snow thickness, and water density and get SIT values which over all compare better to in situ observations than the classical derived SIT product from Hendricks et al. (2021). The better SIT values from Sievers et al. (2023) could either be due to successful FB assimilation, correcting known

https://doi.org/10.5194/tc-2023-122
Preprint. Discussion started: 14 August 2023

biases (Willatt et al., 2011; Kwok, 2014; King et al., 2018) in the CryoSat-2 FB retrials, due to better snow thickness and sea ice density values or due to both. Sievers et al. (2023) links some of the skill of the assimilation to correction of FB through the assimilation. Several studies however have found that snow thickness and sea ice density contribute significantly to SIT biases in the FB to SIT conversion (Alexandrov et al., 2010; Kern et al., 2015; Jutila et al., 2021). recent studies have shown that modelled snow thickness can give good results, substituting the commonly used W99 snow thickness (Landy et al., 2022; Fiedler et al., 2022). Sievers et al. (2023) was the first to use modeled sea ice density values. The values have not yet been evaluated. This paper will address this gap and compare not only the sea ice density but also the snow thickness and water density values from Sievers et al. (2023) with independent observations and values used in the classically derived SIT retrieval from Hendricks et al. (2021). Further, a spatial comparison between the values from Sievers et al. (2023) and Hendricks et al. (2021) is used to determine the influence of the parameters on the SIT conversion in different regions.

Sievers et al. (2023) uses water density values from an ocean model. Uncertainties introduced by water density are by many CryoSat-2 SIT products neglected (Kurtz et al., 2013; Tilling et al., 2018; Hendricks et al., 2021) under the assumption that a single value can be used with an uncertainty of $\pm$ 0.5 kgm^{-3}. Alexandrov et al. (2010) states that the surface water density only varies with 2 kgm^{-3}, which is not reflected in our model results. This is why we decided to include the surface water density in our evaluation as well, even though other studies (Kurtz et al., 2013; Tilling et al., 2018; Hendricks et al., 2021) neglect its influence on the FB to SIT conversion.

2 Data and Methods

2.1 Model data

The sea ice model run in this study is the same as the model used in (Sievers et al., 2023) to assimilate the CryoSat-2 FB. It is a coupled sea ice ocean model, which consist of NEMO v4.0 (Madec et al., 2017) as the ocean component and CICE v6.2 (Hunke et al., 2021) as the sea ice component. The model set up used in this study will be called C6N4 in the following. The NEMO setup closely follows Hordoir et al. (2022) with minor changes to the setup to be run with NEMO v4.0. The atmospheric forcing applied is ERA5 (Hersbach et al., 2017) with a frequency of 3 hours. More details on forcing and setup can be found in (Sievers et al., 2023). The variables discussed in this study are the sea ice density, the water density and the snow thickness. The sea ice density is modelled following:

$$\rho_i = a_b * \rho_b + (1. - a_b) * \rho_{fresh} \tag{2}$$

Here a_b is the fraction of brine contained in the sea ice volume and ρ_b the density of the brine following Assur (1958). This calculation is only available if the mushy ice thermodynamics are used in CICE. ρ_{fresh} is constant and set to $882 kgm^{-3}$.

In CICE, the surface water density is calculated from sea surface salinity following Feltham et al. (2006). This is the CICE default setting.

The snow thickness is calculated by CICE depending on the snow forcing from ERA5. Even though the forcing is the source of the C6N4's snow volume, we found that the atmospheric boundary layer scheme and the atmospheric drag formulation has

https://doi.org/10.5194/tc-2023-122
Preprint. Discussion started: 14 August 2023

a significant impact on the snow thickness. In this study, we used the CICE default atmospheric boundary layer and the form drag formulation from Tsamados et al. (2014).

2.2 AWI data

The weekly CryoSat-2 derived SIT data version 2.4 developed at the Alfred Wegener Institute (AWI) includes all values used for deriving the SIT from radar FB at the corresponding location. The dataset follows the classical approach of deriving SIT from FB, which assumes hydrostatic balance and sea ice density and snow thickness values that depend on the ice type, as described in the introduction. Ice type data used is the OSISAF daily ice type product OSI-403-d (SAF, 2017). The sea ice density values used are $916.7 \pm 35.7 kgm^{-3}$ for FYI and $882 \pm 23\ kgm^{-3}$ for MYI following Alexandrov et al. (2010). The snow thickness used is a combination of the W99 snow climatology and snow thickness product using the Advanced Microwave Scanning Radiometer 2 (AMSR2) in the marginal ice zones. The snow thickness products are weighted depending on location. In the central Arctic extending to the Russian, the Greenlandic and Canadian coast the W99 climatology is dominating. In the marginal ice zones of the Canadian Archipelago, the Fram Strait, the Barents Sea and the Bering Sea the AMSR2 snow thickness is dominating. Following Kurtz and Farrell (2011) they reduce the W99 snow thickness by 50% over FYI. The value used for the water density is 1024 kgm^{-3}, and its uncertainties are neglected (Hendricks et al., 2021). Additional information is available in Hendricks et al. (2021).

2.3 Validation data

2.3.1 Snow

To validate the C6N4 and AWI snow thickness, the altimetric based snow thickness product (ASD) Garnier et al. (2021) from Laboratoire d'Etudes en Géophysique et Océanographie Spatiales (LEGOS) was used. The ASD product is based on the assumption of different penetration depth of different radar wavelengths. It is derived by subtracting the SARAL/Altika Ka-band and CryoSat-2 Ku-band radar height measurements from one another. In its validation study, it was shown that the ASD data product compares better to NASA Operation IceBridge airborne snow thickness observations than both the W99 climatology and the AMSR2 based data product (Garnier et al., 2021). The ASD data product covers the Arctic up to 81.5 ° N. Therefore, the comparisons of both the AWI snow data and the C6N4 snow data was limited to the same geographical extent.

2.3.2 Sea ice density

The sea ice density used for validation is a sea ice bulk density derived from airborne observations described in Jutila et al. (2021). The density was calculated based on the Archimedes' principle following:

$$\rho_i = \rho_w(1 - \frac{H_{fs}}{h_{tot} - H_s}) + (\rho_w - \rho_s)\frac{H_s}{H_{tot} - H_s} \quad (3)$$

They set ρ_w to 1024 kgm^{-3} and ρ_s to 300 kgm^{-3}. The values for H_s (snow thickness), H_{tot} (total snow and ice thickness) and H_{fs} (snow freeboard) are based on airborne observations in the beginning of April 2017 and 2019. The locations of the

https://doi.org/10.5194/tc-2023-122
Preprint. Discussion started: 14 August 2023

field campaign of 2017 are marked in figure 1 by blue dots and stars, and by red dots and stars for the 2019 campaign. H_s was measured with a snow radar similar to those used during the Operation IceBridge campaigns (MacGregor et al., 2021). h_{tot} was measured with an electromagnetic induction sounding instrument also called the EM-Bird, further described by Haas et al. (2009). H_{fs} was measured with a near-infrared, line-scanning Riegl VQ-580 airborne laser scanner. More details about each of the measurements can be found in Jutila et al. (2021). The resulting data includes an error estimate, which was used to filter the data. No values with error larger than 30 kgm^{-3} were used. A second sea ice density data set was used for comparison, obtained

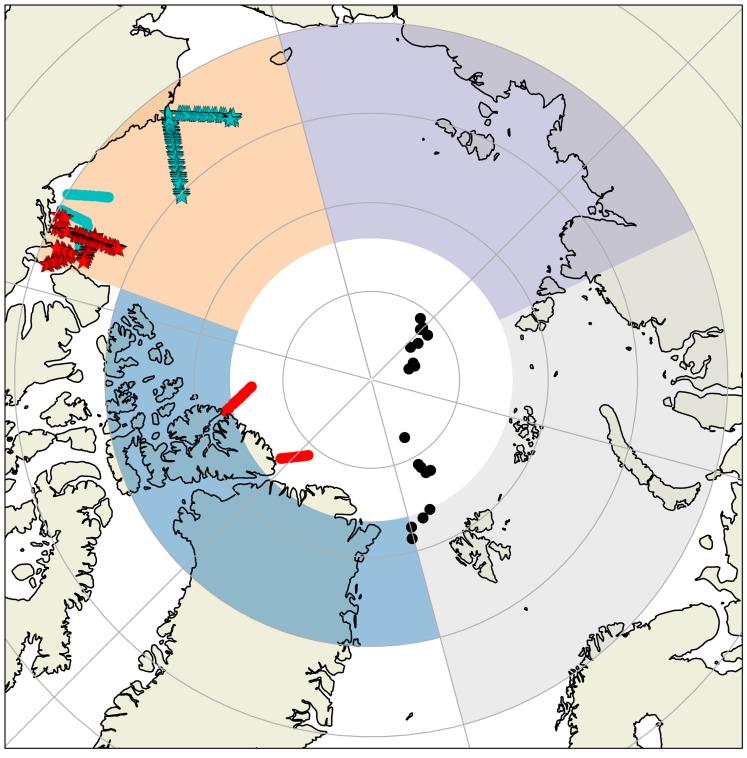

Figure 1. Map showing the locations of the IceBird campaign from 2017 (turquoise stars and dots), 2019 (red stars and dots) and the four areas considered in figure 2. The stars and dots refer to the data marked with stars and dots in figure 4. Region 1 is the region called Canadian Arctic, region 2 is the region called Beaufort Sea, region 3 is the region called Russian Arctic East and region 4 is called Russian Arctic west. The black dots indicate the locations of the MOSAiC core sea ice density measurement shown in figure 5

.

primarily in the central Arctic. This data set was collected during the Multidisciplinary drifting Observatory for the Study of Arctic Climate (MOSAiC) expedition, where sea ice density from FYI ice cores was obtained (Oggier et al., 2023). The sea ice density values were calculated using the method of hydrostatic weighing, which according to Pustogvar and Kulyakhtin (2016) is the most reliable method to measure sea ice density. For this method, the mass of the ice core is measured both in air and in an unspecified liquid (Oggier et al., 2023). The density is given per segment of the measured core, and we calculated

https://doi.org/10.5194/tc-2023-122
Preprint. Discussion started: 14 August 2023

the thickness weighted mean density of the ice core to compare it to C6N4. The location of the coring site was interpolated to the model grid using the nearest neighbor method. The time the measurements were taken range from October 2019 to August 2020. To be able to use the full data set, the 10 year C6N4 original run was extended by 8 months. This period was only used for the comparison of the sea ice density measurements of Oggier et al. (2023).

2.3.3 Water density

The surface water density was calculated from the salinity of the World Ocean Atlas 2018 (WOA) data set (Zweng et al., 2019). The WOA is quality controlled and interpolated to a standardized depth grid. It is the largest freely available gridded data set of oceanographic observations (Boyer et al., 2018). The data set used in this study is the 0.25 ° data set spanning the years 1955 to 2017 and the averaged monthly subsets for October to March. The density was calculated following the salt water density calculation from Feltham et al. (2006) utilizing only the surface values from the WOA data set. The method to calculate the water density from Feltham et al. (2006) was chosen to be in line with the way C6N4 calculates surface water density.

2.4 SIT comparison

One objective of this study is to evaluate SIT differences resulting from the sea ice density, snow thickness and water density differences of the AWI and the C6N4 data. To evaluate this first the mean C6N4 and AWI values for sea ice density, snow thickness and water density had to be calculated. The AWI data was biliary interpolated onto the model grid. All grid points covered by at least 50 satellite overflights were found, and only grid points and time steps covered by both the AWI data product and C6N4 were considered. In a second step, the mean absolute difference (MAD) between the selected C6N4 and AWI values were calculated for each gird cell fulfilling the above-mentioned conditions.

The MAD and mean values are used to determine the mean SIT error as a result of the variation of the parameters of snow thickness and sea ice density. The water density will be treaded slightly differently due to the single value used in the AWI data. To determine the resulting SIT difference from snow thickness and sea ice density, a variation of equation 1 is calculated in each grid cell. For example, for ρ_i this would look like:

$$SIT_{+\frac{1}{2}MAD_{\rho_i},-\frac{1}{2}MAD_{\rho_i}} = \frac{FB\rho_w}{(\rho_w - (\rho_i \pm \frac{1}{2}MAD_{\rho_i}))} + \frac{H_s\rho_s}{(\rho_w - (\rho_i \pm \frac{1}{2}MAD_{\rho_i}))} \tag{4}$$

$$SIT_{\rho_i} = SIT_{+\frac{1}{2}MAD_{\rho_i}} - SIT_{-\frac{1}{2}MAD_{\rho_i}} \tag{5}$$

In equation 4 H_s, ρ_i and ρ_w are the mean values from the C6N4 and AWI data, calculated as described above. The mean FB values are calculated from AWI data only, and the ρ_s values are equal in both data sets. To calculate the SIT difference resulting from the snow thickness difference H_s was varied by $\pm\frac{1}{2}MAD_{H_s}$.

For the water density a similar analysis was conducted, but instead of deriving the mean ρ_w from the C6N4 and AWI values the WOA values were used as the mean ρ_w in equation 4, and the variation $\pm\frac{1}{2}MAD_{\rho_w}$ is given by the difference between

https://doi.org/10.5194/tc-2023-122
Preprint. Discussion started: 14 August 2023

1024 kgm^{-3} for the AWI data, and the WOA values and a winter month (November to April) C6N4 water density climatology calculated from the 10-year model run.

2.5 Probability Density Function

The snow thickness data sets from C6N4, AWI and ASD come in varying spacial and temporal resolutions. The C6N4 data comes on a 10x10 km grid at a weekly frequency, the AWI data covers ca 100 overflights per week, not covering any area above 88°N, and the ASD data comes at a monthly frequency, covering only areas up to 81.5°N. To ensure a fair comparison, the data was divided into 4 regions displayed in figure 1, and the probability density functions (PDF) of each month in each region were calculated for each of the data sets. The PDF indicated the probability of the snow having a certain thickness. The integral of a PDF is always 1, what makes it suitable to compare variables with different temporal and spatial resolutions.

3 Results

3.1 Snow thickness

Figure 2 displays the PDF of the C6N4, AWI and ASD snow thickness data for the month November to March. Compared to the AWI and ASD snow thicknesses, the C6N4 values are the thinnest in November and experience the largest accumulation over the winter season. The largest snow accumulation in the C6N4 data can partly be explained by the fact that the densification of snow is not included in the model. The AWI snow thickness PDFs show distinct peaks resulting from the climatology values. Two, or in some areas even three, peaks are visible. The AWI product includes thinner snow covers over FYI and thicker over MYI, leading to the two peaks. In the Canadian Arctic, three peaks are visible. This is due to varying snow conditions in the included regions, which are separated by the Islands in the Canadian archipelago and Greenland. Overall, the PDFs in

Table 1. Overview of the disagreement between the PDFs in figure 2 using the ASD observations as reference. The disagreement is given as a number between 0 and 2; 0 indicating perfect agreement and 2 indicating absolute disagreement. The background color of the entries indicated which data set agreed better with the observations. The orange fields indicate better agreement between the AWI data set and the ASD snow thickness, and the turquoise fields better agreement between C6N4 and the ASD snow thickness. The intensity of the color indicate the difference between the C6N4 and AWI disagreement.

Month	Canadian Arctic		Beaufort Sea		Russian Arctic East		Russian Arctic West	
	C6N4	AWI	C6N4	AWI	C6N4	AWI	C6N4	AWI
November	0.91	0.58	0.45	0.87	0.3	0.98	0.48	0.98
December	0.54	0.71	0.42	0.84	0.24	1.11	0.22	0.86
January	0.46	0.65	0.25	0.98	0.33	1.28	0.50	0.88
February	0.22	0.78	0.26	1.18	0.61	1.38	0.87	0.62
March	0.26	0.74	0.46	1.24	0.67	1.15	0.94	0.57

figure 2 show that the snow cover of C6N4 seems to be in better agreement with the ASD snow estimate when compared to

https://doi.org/10.5194/tc-2023-122
Preprint. Discussion started: 14 August 2023

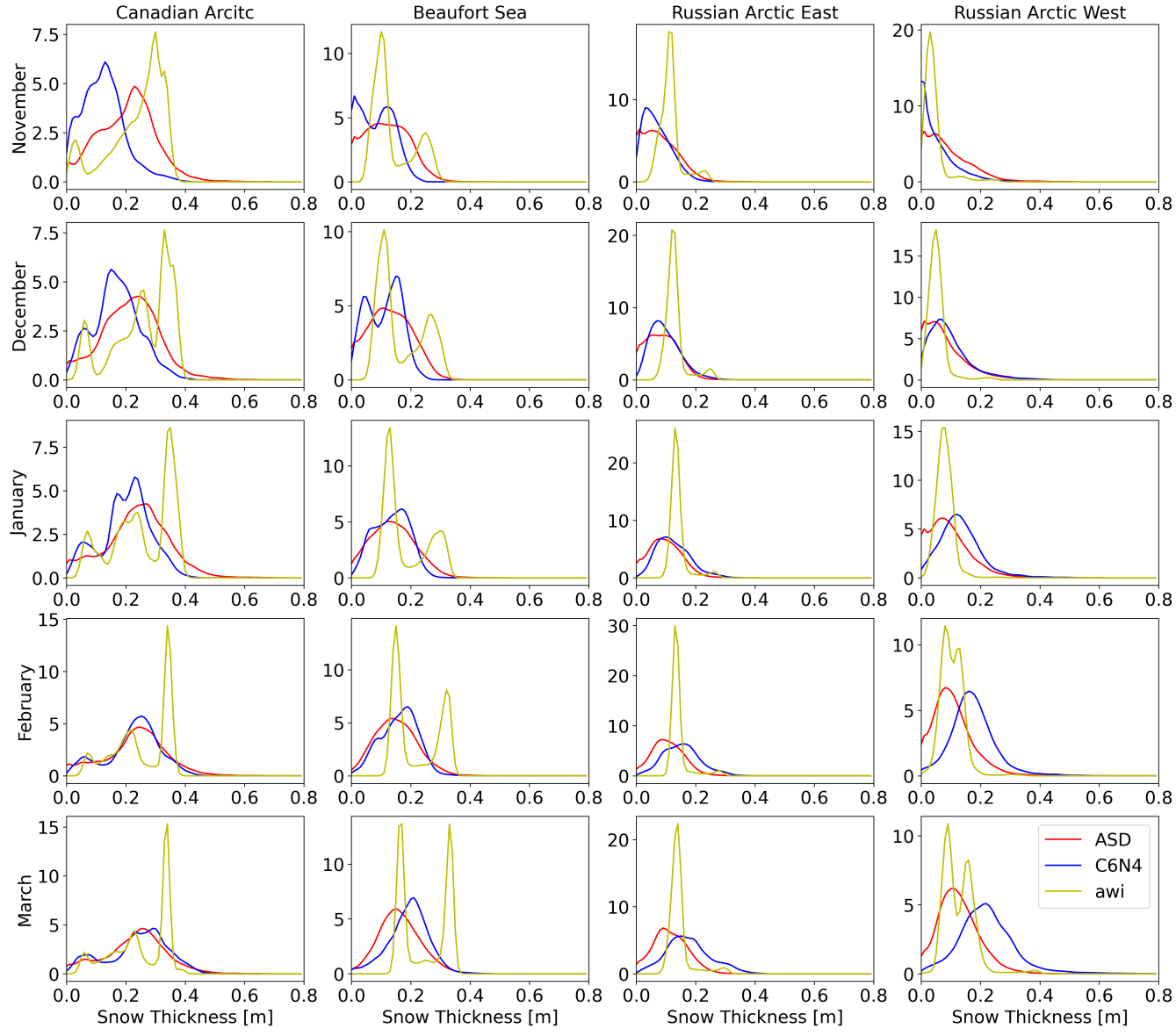

Figure 2. probability density functions for snow in regions where all three data sets exists. Blue lines show the snow thickness used in the AWI data, red lines show ASD based snow thickness, and the turquoise lines show C6N4 snow thickness.

the agreement between the AWI and the ASD estimates. To quantify this, the disagreement between the AWI data and the ASD PDFs and the disagreement between the C6N4 data and the ASD PDFs was calculated and displayed in table 1. The disagreement was calculated as the sum of the integral of the ASD PDF and the integral of the AWI or C6N4 PDF, minus the integral of the area where the two PDF's overlap. The background color of each entry indicates which data set matches better with the ASD. The orange background indicates that the AWI data matches better, and the blue color indicates that the C6N4

https://doi.org/10.5194/tc-2023-122
Preprint. Discussion started: 14 August 2023

data matches better. Most of table 1 is blue, indicating that C6N4 snow indeed compares better to ASD snow than the AWI snow does. Only in the Canadian Arctic the AWI data match better with the ASD data in November, and in the Russian Arctic west the AWI data match better in February and March. The intensity of the background color indicates the magnitude of the differences of the AWI and C6N4 disagreement. Particularly in the Beaufort Sea and the Russian Arctic East, C6N4 matches the ASD data better than the AWI data matches the ASD data. Figure 2 shows that the large disagreement in the Beaufort Sea is created by the presence of a large peak of thick MYI snow ($\sim$ 30-40 cm) in the AWI data in all regions, which is not reflected in the ASD data set, nor in the C6N4 data.

It is clear from figure 2 and table 1 that the C6N4 and the AWI snow thicknesses are significantly different to one another. To evaluate the impact of the snow difference between the C6N4 and the AWI snow thickness, the SIT difference resulting from the snow difference was derived as described in section 2.4. The resulting SIT difference is shown in figure 3 lower right panel. Figure 3 also shows the mean snow thickness used in equation 4 as H_s in the lower left panel, the half MAD used in equation 4 as $1/2\ MAD_{H_s}$ in the lower middle panel, the mean C6N4 snow thickness (upper left), the mean AWI snow thickness (upper middle) and the difference between the mean AWI snow thickness and the mean C6N4 snow thickness (upper right). The white ring at about 79°N is a result of the CryoSat-2 orbit pattern and the condition that the presence of at least 50 satellite observations in a grid cell are needed to calculate the mean and MAD. Figure 3 lower right panel shows that the SIT difference resulting from the snow thickness difference between C6N4 and the AWI data set result in up to 30 cm SIT difference. This difference is located in the regions north of Greenland and Canada, and between Svalbard and Prince George Land. The difference between C6N4 and the AWI snow thickness in the upper right panel shows that the region north of Greenland and Canada is a result of thicker snow in the AWI data and the difference between Svalbard and Prince George Land a result of thicker snow in the C6N4 data.

The region between Svalbard and Prince George Land, which also shows up to 30 cm SIT differences in figure 3 upper panel right, is a result of thicker snow in C6N4, as shown by the positive values in the upper right panel. The disagreement in table 1 values for the Russian Arctic west show that the C6N4 values agree better with the ASD values in November, December and January and the AWI values agree better with the ASD values in the month February and March. The higher miss match in the AWI data in November, December and January is a result of a more uniform snow thickness as shown in the right column in figure 2. The higher disagreement in February and March between C6N4 and the ASD data is caused by overestimation of the snow thickness by the model.

The AWI mean snow thickness in the upper middle panel in figure 3 shows a mean snow thickness in the region east of Greenland of about 20 to 25 cm. The left column in figure 2 shows the PDF for parts of the region north of Greenland and Canada. Above, we discussed that the three peaks in the PDFs are probably a result of different snow thicknesses in the different regions. The AWI mean snow thickness in the upper middle panel in figure 3 shows about 5 to 10 cm difference in the Baffin Bay, which correspond to the first peak in the left column in figure 2, about 15 to 25 cm in the Greenland Sea, which correspond to the second peak and about 35 cm in the region north of Greenland corresponding to the third peak. The disagreement in table 1 shows that the snow thickness of C6N4 in this area only agrees slightly better with the ASD data than the AWI data with the ASD data. The PDF in the left column of figure 2 shows that the agreement between the AWI and ASD data mainly

https://doi.org/10.5194/tc-2023-122
Preprint. Discussion started: 14 August 2023

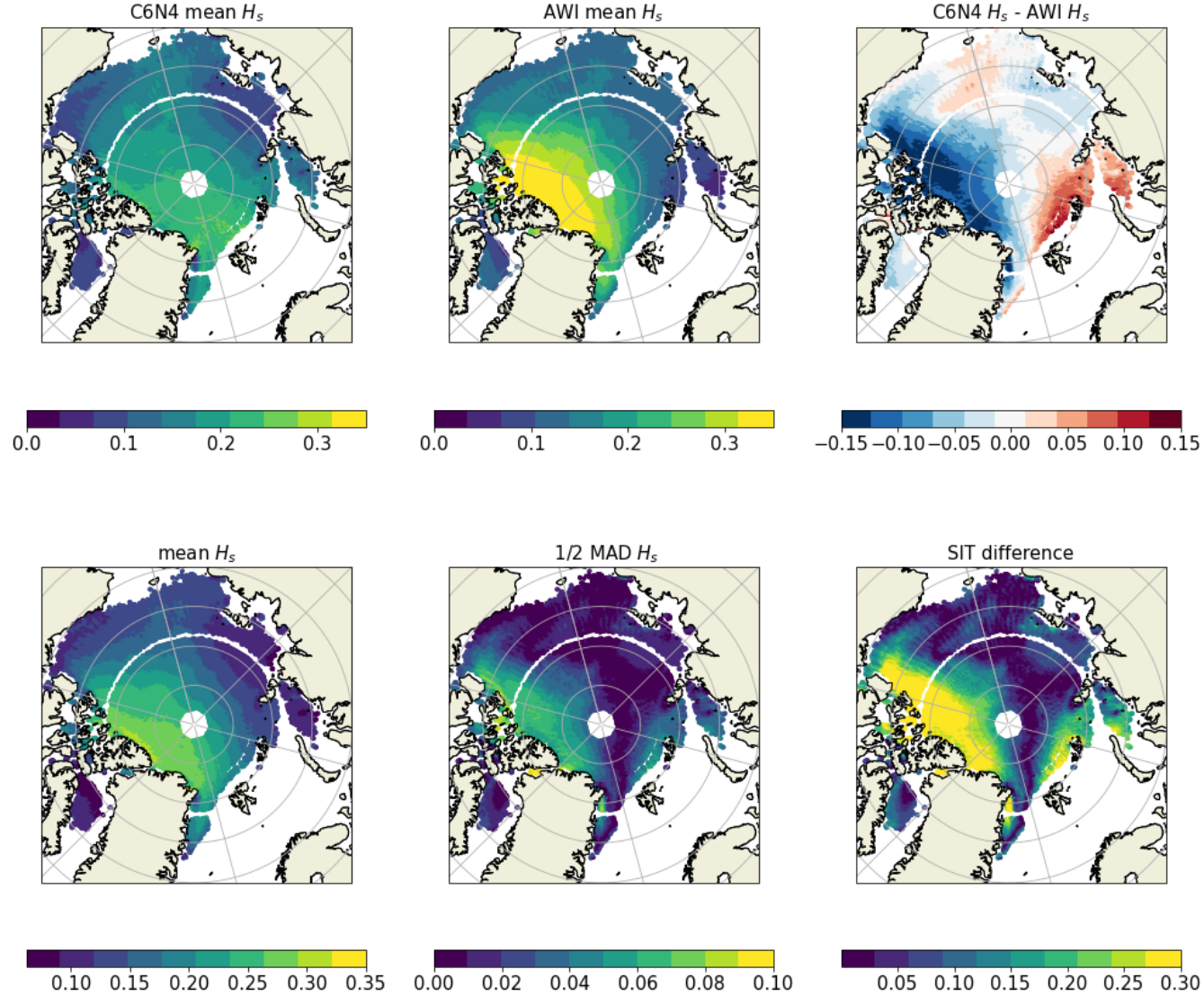

Figure 3. Snow and ice thickness differences between the C6N4 and the AWI data set. The upper left panel shows the C6N4 mean snow thickness, the upper middle panel the AWI mean snow thickness, the upper right the C6N4 - AWI snow thickness difference, the lower left the AWI and C6N4 mean snow thickness used in equation 4 as H_s, the lower middle panel the 1/2 MAD between the C6N4 and the AWI snow thickness and the lower right the resulting sea ice thickness difference.

results as an agreement between the two first peaks. To validate this, the disagreement between the region north of Greenland and Canada was calculated, excluding the Baffin Bay and Greenland Sea. The resulting disagreement values are displayed in table 2. The disagreement for both the AWI data and the C6N4 data is increased in table 2 in comparison to the first column in table 1. The results in table 2 show that the disagreements in November, December and January does not change significantly.

https://doi.org/10.5194/tc-2023-122
Preprint. Discussion started: 14 August 2023


The Cryosphere Discussions

Table 2. Disagreement between the AWI and ASD, and C6N4 and ASD snow thickness excluding Baffin Bay and Greenland Sea from the Canadian Arctic region.

Month	Canadian Arctic	
	C6N4	AWI
November	1.48	1.24
December	1.14	1.40
January	1.12	1.33
February	0.55	1.50
March	0.26	1.48

The model melts off almost all snow over summer. This results in too thin snow in the beginning of winter. The ASD snow only changes slightly over the winter in the Canadian Arctic region, while the third peak of the AWI snow is spread slightly wider from November and gains more and more snow of about 38 cm over the winter. This is visible in figure 2, but even more pronounced in the analysis of the reduced Canadian Arctic region listed in table 2.

The mean snow thickness in the upper left and middle panel of figure 2 shows not only that the C6N4 snow thickness is over all thinner than the AWI snow thickness, but also that the snow thickness has different distributions. The thickest snow in C6N4 north of Greenland is located further east than in the AWI data. The thinnest snow in C6N4 is located in the eastern Beaufort Sea and in the Laptev Sea, while it is located in the Barents Sea in the AWI data.

3.2 Sea ice density

The relation between the sea ice density retrievals from the IceBird measurements of Jutila et al. (2021) and the C6N4 and AWI data is displayed in figure 4. According to Jutila et al. (2021) the observations from 2017 were taken over FYI locations, while the 2019 observations cover both MYI and FYI areas. To distinguish the two data sets, they were shown in two separate panels. All IceBird measurements originating from the same day and grid cell were averaged to one value. Grid cells with less than 10 IceBird measurements were excluded (0.9 % of the data) from the analysis. The correlation coefficients and RMSD between the IceBird and AWI, and IceBird and C6N4 data are listed in table 3 for each year separately. In both 2017 and 2019 there appear to be clustering in C6N4 and AWI data. The flight paths of the expedition in figure 1 in both years are located in

Table 3. Correlation coefficients between C6N4 and the IceBird sea ice density and between the AWI and IceBird data, as displayed in figure 4.

	2017		2019	
	C6N4	AWI	C6N4	AWI
R value	0.42	0.37	0.42	0.24
RMSD	35	35	25	22

https://doi.org/10.5194/tc-2023-122
Preprint. Discussion started: 14 August 2023

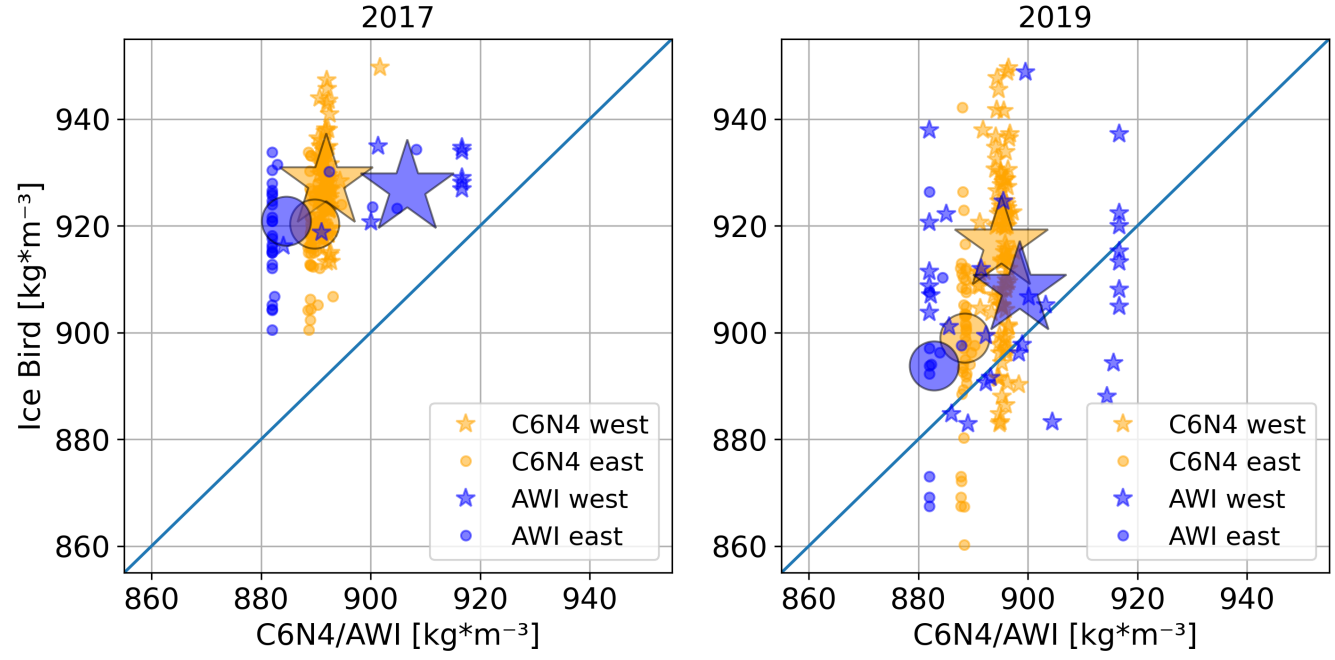

Figure 4. The IceBird sea ice density plotted against AWI (blue) and C6N4 (orange) sea ice densities. The stars and dots represent the Western and Eastern observation sites respectively, and the large symbols with black outline are the mean values for each region.

two different locations. The clustering is a result of the different representations of sea ice densities in C6N4 and the AWI data at the different locations, which are marked by stars and dots, where the stars represent the eastern locations (also marked in figure 1). Since the data is clustered for both the AWI and the C6N4 data, the RMSD was calculated for each location and year.

Both data sets reveal low correlations. The C6N4 data correlates overall better with the IceBird data, with a similar correlation coefficient in both year. In 2017 the AWI data correlates better with the IceBird data than it correlates in 2019. The RMSD between the IceBird and AWI sea ice density is lower than between IceBird and C6N4 sea ice density. In general, the IceBird observations of sea ice densities are higher than both the C6N4 and the AWI data.

According to Jutila et al. (2021) the IceBird observation data includes both MYI and FYI in the 2019 measurements, but only FYI in the 2017 measurements. The FYI sea ice density value for the AWI data is 917 kgm^{-3}. The majority of the AWI sea ice densities (blue points) in figure 4 left panel show, however, a typical MYI sea ice density value of 882 kgm^{-3} for the year 2017. The C6N4 data is also less dense in 2017 than in 2019 indicating that there is more MYI in 2017 than in 2019 in contradiction to the IceBird observations. The large stars and dots with black outlines in figure 4 show the mean of the C6N4 and AWI sea ice densities, respectively. The locations of these stars and dots show that the AWI data and the C6N4 data agree at least to some extent on which regions are lighter and denser.

https://doi.org/10.5194/tc-2023-122
Preprint. Discussion started: 14 August 2023

In the 2019 plot (figure 4 right-hand panel), the mean IceBird values (large stars and dots) differ. This is due to the different amount of data points covered by the AWI data and C6N4 data. The comparison with the AWI data only takes into account the values covered by a CryoSat-2 overflight.

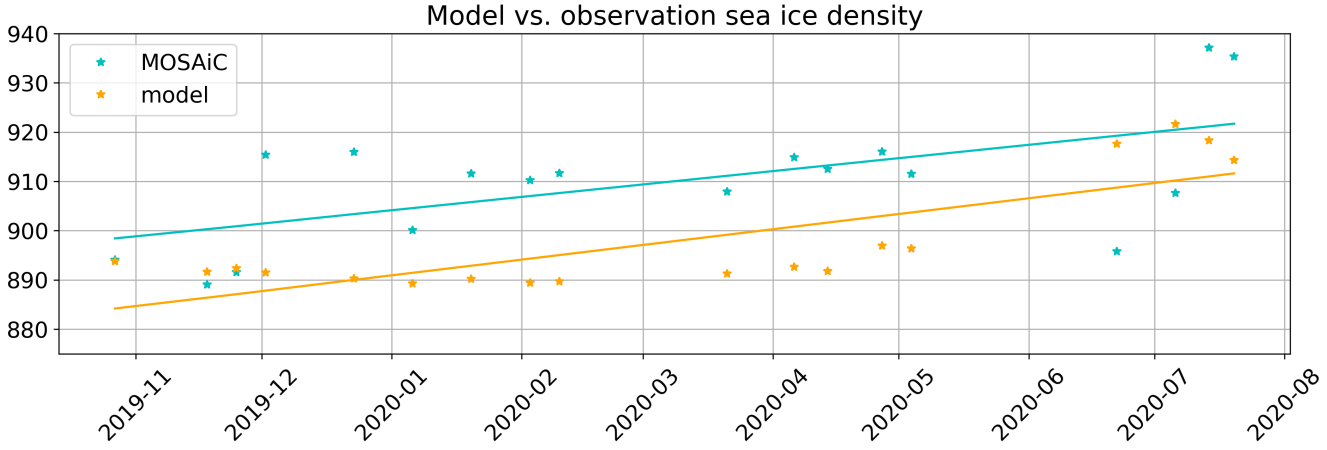

Figure 5. C6N4 sea ice density estimates and MOSAiC FYI core sea ice density.

To include a data set in which the seasonal cycle of the sea ice density is reflected, a comparison has been made between the sea ice core based sea ice density measured during the MOSAiC expedition and the model based estimates. Both the MOSAiC density measurements and the C6N4 density estimates are plotted against time in figure 5. Similar, as observed in the comparison to the IceBird observations, figure 5 shows that the C6N4 estimates are in general lighter than the observations. In regard to the seasonal cycle, figure 5 shows that both densities increase with time. The linear regression of the C6N4 values is slightly steeper than the observation's. The observations show higher variability than the C6N4 values. This can be explained with the fact that the observations are taken in one particular point on the same ice floe, whereas C6N4 represents a 10x10 km averaged value. The AWI values are not shown in the figure since the values are constant equal to 882 kgm^{-3} and the AWI locations coincided with the MOSAiC observations in only four locations.

The RMSD between the C6N4 sea ice density and MOSAiC observations equals 18 kgm^{-3}. Calculating the RMSD between the MOSAiC data and a constant value of 882 kgm^{-3}, results in a RMSD of 31 kgm^{-3}. The RMSD between the C6N4 and the MOSAiC data is 13 kgm^{-3} lower than the RMSD between the AWI single value and the MOSAiC observations. In figure 6 the C6N4 mean sea ice density is shown in the upper right panel, whereas the AWI mean sea ice density is shown in the upper middle panel and their differences in the upper right panel. Overall, the AWI values are denser in most regions in the Arctic, except in the region north of Greenland and Canada. In most regions of the Arctic, the AWI data is either 882 kgm^{-3} (MYI areas) or 917 kgm^{-3} (FYI areas). The difference between the C6N4 and the AWI data shows that the typical MYI areas (north of Greenland and Canada) are denser in C6N4 and the typical FYI areas are denser in the AWI data. Figure 6 shows the mean sea ice density between the C6N4 and AWI data in the lower left panel, half a mean absolute difference in the lower middle panel and the difference in SIT in the lower right panel. The largest SIT differences as seen in figure 6 lower right panel

https://doi.org/10.5194/tc-2023-122
Preprint. Discussion started: 14 August 2023

are located in a band spanning from the Greenland Sea, north along the Russian side of the central Arctic to the East Siberian
275 Sea. Comparing the locations of this maximum SIT differences with the MAD values in the lower middle panel shows that the largest differences in MAD do not exactly coincide with the largest SIT differences in the lower right panel. This shows that in this region the SIT is more sensitive to sea ice density variations than in others. The lowest MAD in the lower middle panel

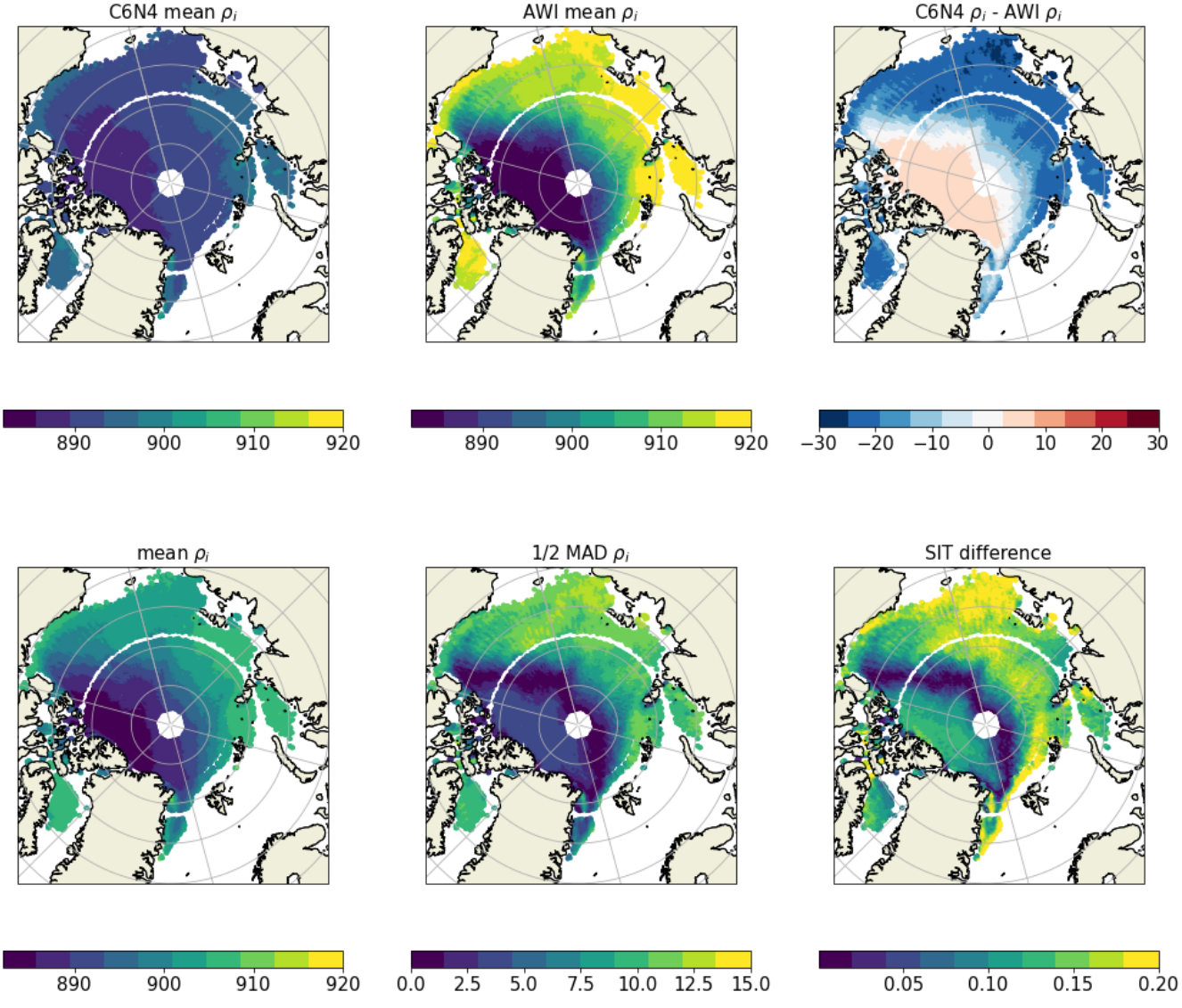

Figure 6. Sea ice density and ice thickness differences between C6N4 and the AWI data set. The upper left panel shows the C6N4 mean sea ice density, the upper middle panel the AWI mean sea ice density, the upper right the C6N4 - AWI sea ice density difference, the lower left the AWI and C6N4 mean sea ice density used in equation 4 as ρ_i, the lower middle panel the 1/2 MAD between the C6N4 and AWI sea ice density and the lower right the resulting sea ice thickness difference.

https://doi.org/10.5194/tc-2023-122
Preprint. Discussion started: 14 August 2023

in figure 6 is located in the region north of Greenland and Canada. By comparing the SIT differences in this region with the SIT differences in the Laptev Sea shows that they are about the same, even though the ρ_i MAD is about twice as large in the Laptev Sea compared to the region north of Greenland and Canada. This shows that the sea ice density in the region north of Greenland and Canada are more important when deriving the SIT than in the Laptev Sea.

3.3 Water density

In the left panel of figure 7 the WOA water density averaged over the months November to March is displayed and in the second panel to the left the 10-year C6N4 mean water density is displayed. The middle panel shows the WOA mean water density minus the AWI water density of 1024 kgm^{-3} and the WOA mean water density minus the 10-year mean C6N4 water density in the second panel from the right. The right panel in figure 7 shows the difference between the AWI single value and the C6N4 water density. Comparing the differences between the WOA data, the C6N4 and the AWI data, it shows that the C6N4 data agrees better with the WOA climatology than the single value from the AWI data, but is still less variable when compared to the variability of the WOA data. The standard deviation (STD) between the C6N4 and the WOA water densities for the entire Arctic is 1.6 kgm^{-3} and the STD between the WOA and the AWI water densities is 2.1 kgm^{-3}. To evaluate whether the differences in water density leads to significant differences in SIT, or can be neglected as done in most CyoSat-2 SIT data sets, we calculated the SIT differences with varying water densities (ρ_w). How the SIT difference was calculated is described at the end of section 2.4. The results are shown in figure 8. The displayed SIT differences vary between 0 and 7.5 cm for both data sets. The SIT calculated from the WOA-AWI density has a more wide-spread variation than is the case for the one calculated from WOA-C6N4. The C6N4 and AWI water density lead to thicker ice in the region north of Greenland and Canada and thinner ice in the Greenland Sea. In the Russian shelf region, the AWI data leads to thicker ice and the C6N4 data to thinner ice. The SIT difference from the AWI data in the Russian shelf region is more pronounced when compared to the difference from the C6N4 data.

4 Discussion

4.1 Snow thickness

By comparing the modelled, the AWI, and the ASD snow thicknesses in figure 2 and table 1, we find the best agreement between the C6N4 snow thickness and the ASD snow thickness. The AWI snow thickness is in general too thick. The AWI snow thickness consist of two snow products: The W99 climatology and the AMSR2 snow thickness product. The areas compared in this study almost all fall into the area where the W99 climatology is used, except in the Greenland Sea and the Baffin Bay. The snow thickness comparison in figure 2 does not include any snow observations in the central Arctic. Zhou et al. (2021) compares eight different snow thickness products including snow thickness values in the central Arctic to W99 and finds, that W99 is significantly thicker than all of them. This is in good agreement with our results.

https://doi.org/10.5194/tc-2023-122
Preprint. Discussion started: 14 August 2023

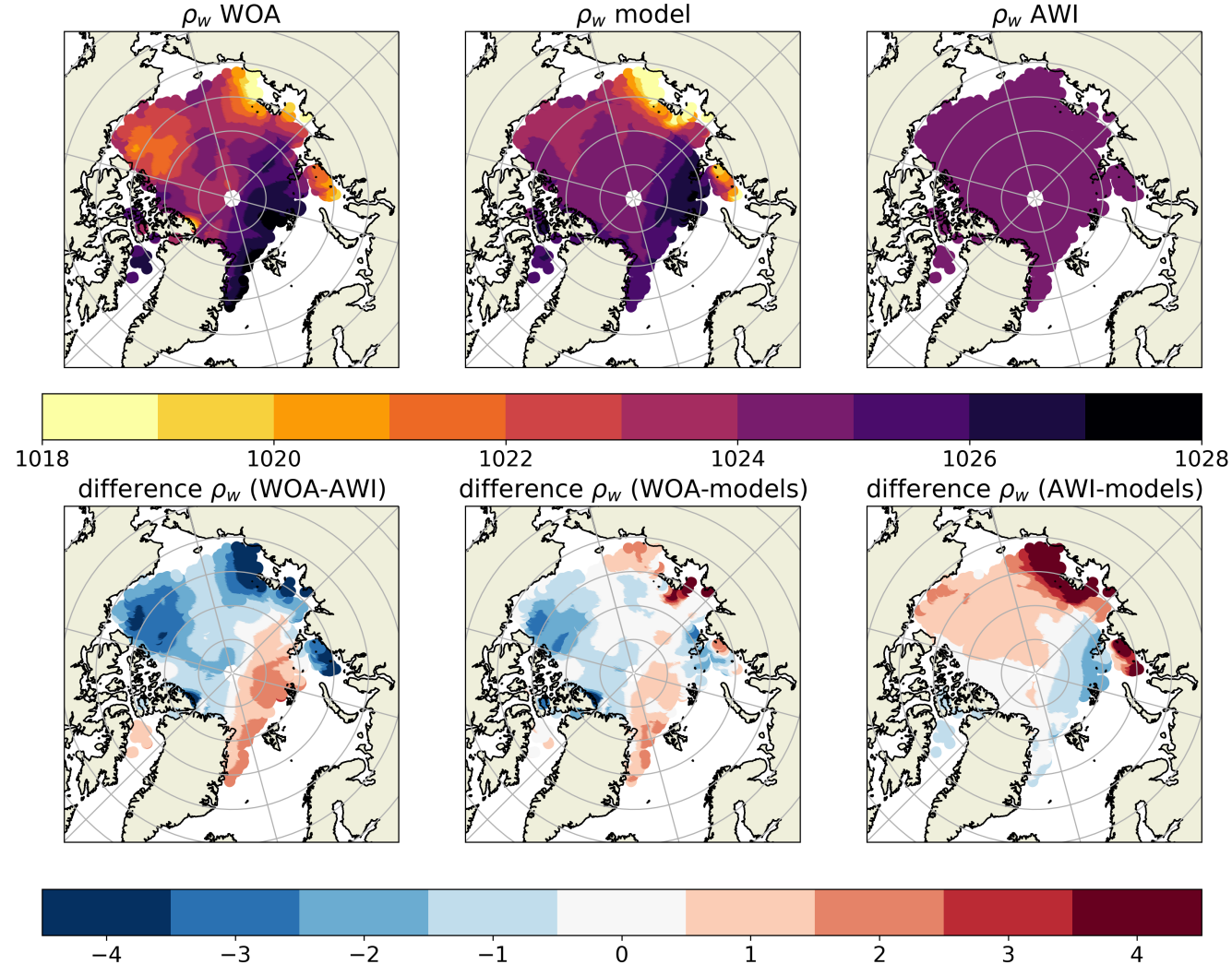

Figure 7. From left to right: The WOA water density, the C6N4 water density, the difference between the WOA and the AWI water density, the difference between the WOA and the C6N4 density and the difference between the AWI and C6N4 water density.

The PDF's in figure 2 show that the C6N4 snow thickness, when compared to the ASD snow thickness product, overall is thinner in the beginning of the winter season and thicker by the end of the winter season. The snow is thinner in the beginning of the winter in C6N4, because most of the snow in the model is melted off during the summer. There are three possible reasons for the thicker snow by the end of winter.

First, C6N4 does not include snow densification, which is the process where wind and temperature reduces the volume over time without changing the mass (Liston et al., 2020). When C6N4 is run with FB assimilation, the value of 0.25 in equation 1 is substituted with a term depending on the snow density, which densifies over the winter season according to a linear function

https://doi.org/10.5194/tc-2023-122
Preprint. Discussion started: 14 August 2023

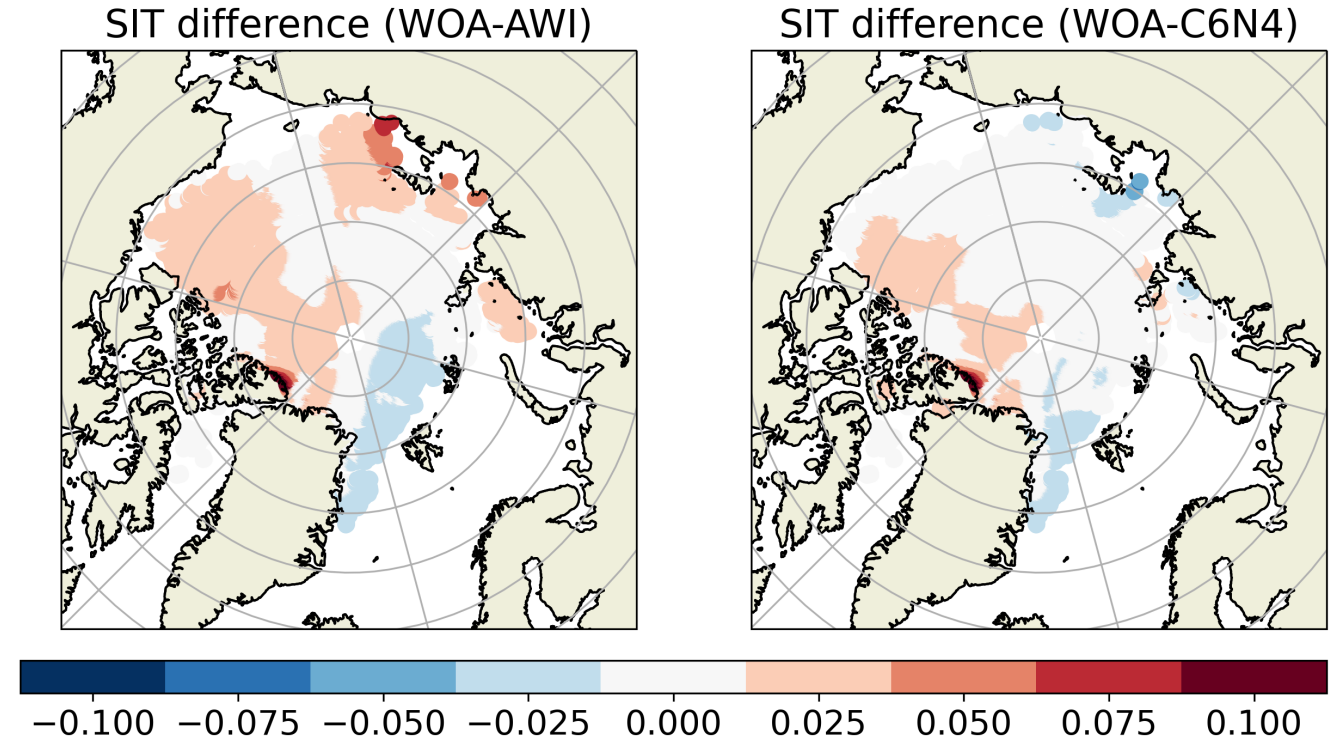

Figure 8. SIT difference, resulting from varying equation 4 by the difference between the C6N4/AWI water density and the WOA water density.

introduced by Mallett et al. (2021). This snow densification term is only used during the assimilation and does not influence the snow thickness anywhere else in the model (Sievers et al., 2023). To avoid overestimation of the snow thickness in late winter, the densification used in the assimilation following Mallett et al. (2021) could be applied to also scale the snow thickness.

The second reason for the difference in snow thickness in late winter could be that the Ku-band radar, which is used to determine the snow-ice interface in the ASD product, does not penetrate the entire snowpack in the late winter months (Willatt et al., 2011; Kwok, 2014; King et al., 2018). In situ observations that can be used to evaluate the Arctic wide snow thickness products are limited in time and space, thus a consistent validation of this will remain a challenge.

A third reason that may bias the C6N4 snow thickness is regional biases in the snowfall from ERA5, which could be overestimated in certain regions. Stroeve et al. (2020) compared two snow model runs forced with ERA5 and NASA's Modern Era Retrospective-Analysis for Research and Applications, Version 2 (MERRA-2) (Gelaro et al., 2017). They find that the modelled snow thickness from both atmospheric forcing data sets are thicker compared to W99 in a similar region, slightly further west. They attribute this difference to a storm that brought more snow into the region in the year they evaluated, but they also mention that the snow fall rate might have changed over the past decades due to changes in the atmospheric circulation as a result of the decreased summer sea ice extent (Stroeve et al., 2011). The in situ observations from the MOSAiC expedition

https://doi.org/10.5194/tc-2023-122
Preprint. Discussion started: 14 August 2023

can provide some insight of the evaluation of at least one winter season. Wagner et al. (2022) compared snowfall rates during the MOSAiC expedition to ERA5 and finds good agreement between the observed and ERA5 snowfall rates. C6N4 is forced by ERA5 snowfall. Further, (Kwok et al., 2020) finds that snow thickness estimates from combined CryoSat-2 and IceSat data compares well with reconstructed snowfall from ERA5. However, they also use the CryoSat-2 radar measurements, which might lead to underestimation of snow thickness, as mentioned above. All of these studies (Stroeve et al., 2011; Zhou et al., 2021; Wagner et al., 2022; Kwok et al., 2020) support the thicker modelled snow in the Russian Arctic west area to be more realistic than both the ASD product and the AWI snow thickness.

Overall, table 1 shows that the snow thickness from C6N4 agrees better with the ASD data product than the AWI snow thickness, except in two regions, where the AWI and the ASD snow products agrees better for limited periods of the year. These regions are the Canadian Arctic and the Russian Arctic West. In the Russian Arctic West, the C6N4 snow thickness increasingly disagrees with the ASD snow thickness in the late winter months. As mentioned above, this could be a result of either the Ku-band radar not penetrating the entire snowpack or the snow in C6N4 not including snow densification. The in situ measurements on which King et al. (2018) base their findings that the Ku-band radar does not penetrate the entire snowpack are taken north of Svalbard, a region included in the Russian Arctic west. In November in the Canadian Arctic, the difference most likely deems from the overestimation of summer snow melt in C6N4. This region is typically covered by ice that has survived several winters. The snow thickness from the snow model in Stroeve et al. (2020) supports the snow thickness of about 20-25 cm from the ASD product in November in the Canadian Arctic. Overall, we conclude that there is enough evidence that the C6N4 snow thickness is more realistic than the AWI data snow thickness.

Figure 3 lower right panel shows that the snow thickness biases on average can lead to a SIT difference of about 30 cm and that this difference is located in the region north of Canada and Greenland and between Svalbard and Prince George Land. As discussed above, there are good reasons to assume that the C6N4 snow thickness reflects the real snow thickness better than the W99 snow thickness, which is the basis for the majority of the AWI snow thickness used in this comparison. Sievers et al. (2023) finds that the assimilated SIT is thinner than the AWI SIT. Since an overestimation in snow thickness leads to an overestimation in SIT, this implies that the thicker snow present in the AWI data can cause this difference.

4.2 Sea ice density

According to figure 4 the C6N4 sea ice density is too low and has too little spatial variability compared to the airborne IceBird observations. The mean C6N4 sea ice density in figure 6 upper left panel supports this finding. Figure 5 also shows that the C6N4 sea ice density is too low when compared to MOSAiC observations, but that the seasonal variability is in good agreement. The linear regression in figure 5 shows that the MOSAiC observations increase with about 20 kgm^{-3} over the period shown, and that C6N4 is capable of modelling this increase. Ji et al. (2021) finds the opposite development of increasingly lighter sea ice from February to August. The difference between the data in Ji et al. (2021) and the MOSAiC observations is that Ji et al. (2021) includes observations from all over the Arctic, while the MOSAiC measurements are obtained in proximity of one another, and thus represent the same ice floe. This indicates that the Arctic wide sea ice density decrease from winter to summer (Ji et al., 2021), but that the particular sea ice floe which was probed during MOSAiC, shown in figure 5 follows a

https://doi.org/10.5194/tc-2023-122
Preprint. Discussion started: 14 August 2023

more local pattern. The fact that C6N4 simulated the local increases in sea density in-line with the observed increase, shows that C6N4 is capable of simulating the temporal development of the sea ice density.

All observations are denser than the C6N4 sea ice density. The formula used to calculate the sea ice density (equation 2) accounts for the amount of brine, but not the fact that the amount of enclosed air bubbles in the ice changes with time. MYI ice was found to contain a significant amount of air bubbles (Timco and Frederking, 1996). The value for ρ_{fresh} is 882 kgm^{-3}, which reflects a typical MYI value (Alexandrov et al., 2010). One suggestion to improve the sea ice density in future models could be to vary ρ_{fresh} depending on the ice age.

Comparing the AWI sea ice density values to the C6N4 and observations in figure 4 shows that the AWI data in comparison to the C6N4 data better reflects the spread of the observed sea ice density, but tends to be too low. This is in line with both Jutila et al. (2021) and Ji et al. (2021), who found that the typical sea ice density values suggested by Alexandrov et al. (2010) are too low. As the Alexandrov et al. (2010) sea ice density values are used in the AWI data set, these findings agree with each other. Figure 6 upper right panel shows that the C6N4 density is slightly higher than the AWI density in typical MYI zones and significant lower in FYI zones. Figure 6 lower right panel shows that the largest difference in SIT are found in the same location as the largest density differences, which is intuitive. Furthermore, the region north of Canada and Greenland gives up to 15 cm SIT differences as a result of only 4 kgm^{-3} difference in sea ice density. For comparison, the Laptev Sea shows similar SIT differences, but the sea ice densities between the data sets differ on average 10 kgm^{-3}, which is more than double the amount when compared to the density differences in the area north of Greenland. Thus, there is a higher sensitivity to the sea ice density variations in the region north of Greenland. This is caused by the fact that the ice in this region is significantly thicker compared to the Laptev Sea, and thus a change in density affects a larger volume of sea ice. We conclude that an accurate sea ice density is particularly important in the region north of Greenland and Canada.

4.3 Water density

The AWI water density is represented by a singular value with no spatial variations. The WOA data varies about 3 kgm^{-3} more in between the regions than the C6N4 data. Following WOA (Figure 7) the general pattern of dense water on the Atlantic side of the Arctic and lighter water in the Russian shelf area and the Beaufort Sea is replicated by C6N4, however the difference is less pronounced in C6N4. Especially the Beaufort Sea surface water is lighter and the Fram Strait region denser in WOA. The largest differences in between the WOA climatology and the C6N4 data is found in the Laptev Sea. The Laptev Sea surface salinity is highly dependent on river run-off and atmospheric forced transport of the river run-off (Janout et al., 2020). Shiklomanov et al. (2021) showed that the river run-off has increased over the past years, which could explain the denser water in the WOA data, as it includes data from the last decades. In most regions of the Arctic, there are less than 50 water density observations on a 1x1 degrees grid for a period of over 150 years (Zweng et al., 2018). Even though, the WOA climatology is compiling a large part of all existing oceanographic observations (Zweng et al., 2018), one has to keep in mind that the coverage is extremely sparse. Keeping all limitations in mind, C6N4 compares better to the WOA data set than the single value used in the AWI data set. The C6N4 water densities might even outperform the WOA climatology in the Russian shelf region due to the inclusion of recent changes in fresh water content in this area from river run-off.

https://doi.org/10.5194/tc-2023-122
Preprint. Discussion started: 14 August 2023

We find that the water density can lead to up to 7.5 cm difference in the derived SIT. All existing SIT data products which are using the hydrostatic balance equation to derive SIT are either neglecting the error contribution from water density (Kurtz et al., 2013; Tilling et al., 2018; Hendricks et al., 2021) or are using values of 0.5 kgm^{-3} (Guerreiro and Fleury, 2017) as the uncertainty with reference to Alexandrov et al. (2010) or Laxon et al. (2003). Alexandrov et al. (2010) refers to three data sources (i.e: Gorshkov (1980); Pavlov and Stanovoy (1998); Timokhov and Tanis (1997)) for their assumptions which were not accessible for us, and Laxon et al. (2003) refers to Wadhams et al. (1992). Wadhams et al. (1992) evaluated the seasonal variability of the Arctic surface water density and finds that it varies by about 0.5 kgm^{-3}, but not the spacial variability. Figure 6 shows that the water density varies by up to 10 kgm^{-3} in space. In general, we recommend using a climatology or model value. If a single value is used for the water density in equation 1, the variability should be accounted for. We suggest, in this case, to use 2.6 kgm^{-3} calculated from the std between the WOA and AWI density of 2.1 kgm^{-3} plus 0.5 kgm^{-3} to account for the seasonal variability, as suggested by Wadhams et al. (1992). Figure 8 shows that using a variable water density can improve the SIT by up to 7.5 cm, which is why we suggest that data products deriving SIT via the hydrostatic balance equation should use a data product like the WOA climatology. As discussed above, the WOA climatology is also associated with its own uncertainties, but these are still smaller than those related to a single value.

The C6N4 water density was calculated following Feltham et al. (2006), which calculates the density only depending on the salinity. This is currently the default in CICE. For consistency, the WOA water density was calculated following Feltham et al. (2006) as well. The oceanographic standard would have been to use the salinity and temperature dependent TEOS-10 (Commission et al., 2015). We tested if using TEOS-10 had given any different results in the SIT difference, or the overall STD calculation between the AWI and WOA data, and found that it would not.

4.4 Evaluation of Sea Ice Thickness differences

Figure 3 and 6 lower right-hand side panels and 8 show the sea ice thickness differences resulting from the different snow thickness, sea ice density and water density values. The largest SIT differences, with 30 cm, result from the snow thickness differences shown in figure 3 closely followed by the ice density with 20 cm. Both the snow and the sea ice density influencing the SIT calculation has been discussed by other studies (Zygmuntowska et al., 2014; Kern et al., 2015; Ji et al., 2021; Jutila et al., 2021). Kern et al. (2015) finds that both snow thickness and sea ice density contribute to the SIT uncertainty to equal parts, while Zygmuntowska et al. (2014) finds that the snow contributes with 70 % and the sea ice density with 30-35 %. Even though this study does not analyze the exact contribution from each parameter in percentage, our finding support Zygmuntowska et al. (2014) finding that the snow thickness has the larger influence.

As mentioned above, variations in water density are in most studies assumed to have no or negligible influence on the SIT calculation (Alexandrov et al., 2010; Kurtz et al., 2013; Guerreiro and Fleury, 2017; Tilling et al., 2018; Hendricks et al., 2021). Figure 8 shows that the sea ice density can lead to up to 7.5 cm difference in SIT, which is little in comparison to the SIT differences initiated by snow thickness and sea ice density, but still not negligible.

https://doi.org/10.5194/tc-2023-122
Preprint. Discussion started: 14 August 2023

5 Conclusions

The first objective of this paper was to evaluate the C6N4 parameters. We find that the C6N4 snow thickness compares well to the ASR snow thickness product, which has been used as reference measurements, except in the beginning of winter, where the C6N4 snow thickness tends to be too thin. Evaluating the C6N4 sea ice density, we found that the C6N4 sea ice density is not variable enough and too light, but has a good seasonality. This could be improved by varying ρ_{fresh} in equation 2. The seasonal variability of the sea ice density compares well to observations (figure 5). The water density shows too little spatial variability compared to the WOA water density, but some of the differences to the WOA reference measurements is likely a result of undersampling. Overall, the C6N4 water density shows similar destitution patterns as the WOA water density.

Comparing the C6N4 parameters to the AWI parameters and observations shows that the C6N4 snow thickness and water density is in better agreement with the observations than the parameters used in the classical derived AWI SIT product. The AWI sea ice density reflects the overall variability better (figure 4), but is in general less dense over typical MYI areas and denser in typical FYI areas.

By comparing the resulting SIT differences, we find that the snow thickness leads to the largest differences by up to 30 cm, followed by the sea ice density resulting in SIT differences by up to 20 cm. The water density is, as expected, the variable with the smallest impact on the estimated SIT. In contrast to other studies, we find that the water density can lead to 7.5 cm difference in the SIT and that the error is not negligible, as commonly assumed (Kurtz et al., 2013; Tilling et al., 2018; Hendricks et al., 2021). To our knowledge, all public available CryoSat-2 SIT products assume a water density uncertainty of 0 to 0.5 kgm^{-3} which is based on assumptions only taking into account the seasonal variability of water density (Wadhams et al., 1992), but not the spatial variability. We suggest changing the sea ice density uncertainty to 2.6 kgm^{-3} to account for both the seasonal and spatial variations, or using water density values from climatologies like the WOA, or as in this study ocean model values.

Author contributions. IS contributed by writing the manuscript and performing all data analysis and model runs. HS advised on CryoSat-2 related topics, edited and reviewed the manuscript and provided general feedback during the preperation of the study. TR advised on model related topics, edited and reviewed the manuscript and provided general feedback on the setup of the study.

Competing interests. To the knowledge of the authors there are no competing interest

Acknowledgements. This study is a collaboration between the Danish Meteorological Institute, Aalborg University and the Danish Technical University. It is funded by the Danish State through the National centre for Climate Research and the Act of Innovation foundation in Denmark through the MARIOT project (Grant Number 9090 00007B).

https://doi.org/10.5194/tc-2023-122
Preprint. Discussion started: 14 August 2023

References

Alexandrov, V., Sandven, S., Wahlin, J., and Johannessen, O.: The relation between sea ice thickness and freeboard in the Arctic, The Cryosphere, 4, 373–380, 2010.

Assur, A.: Arctic sea ice, National Academy of Sciences-National Research Council. Chap. Composition of sea ice and its tensile strength, pp. 106–138, 1958.

Beaven, S., Lockhart, G., Gogineni, S., Hossetnmostafa, A., Jezek, K., Gow, A., Perovich, D., Fung, A., and Tjuatja, S.: Laboratory measurements of radar backscatter from bare and snow-covered saline ice sheets, Remote Sensing, 16, 851–876, 1995.

Boyer, T. P., García, H. E., Locarnini, R. A., Zweng, M. M., Mishonov, A. V., Reagan, J. R., Weathers, K. A., Baranova, O. K., Paver, C. R., Seidov, D., et al.: World Ocean Atlas, 2018.

Commission, I. O. et al.: The International thermodynamic equation of seawater–2010: calculation and use of thermodynamic properties.[includes corrections up to 31st October 2015]., 2015.

Feltham, D., Untersteiner, N., Wettlaufer, J., and Worster, M.: Sea ice is a mushy layer, Geophysical Research Letters, 33, 2006.

Fiedler, E. K., Martin, M. J., Blockley, E., Mignac, D., Fournier, N., Ridout, A., Shepherd, A., and Tilling, R.: Assimilation of sea ice thickness derived from CryoSat-2 along-track freeboard measurements into the Met Office's Forecast Ocean Assimilation Model (FOAM), The Cryosphere, 16, 61–85, 2022.

Garnier, F., Fleury, S., Garric, G., Bouffard, J., Tsamados, M., Laforge, A., Bocquet, M., Fredensborg Hansen, R. M., and Rémy, F.: Advances in altimetric snow depth estimates using bi-frequency SARAL/CryoSat-2 Ka/Ku measurements, The Cryosphere Discussions, 2021, 1–40, https://doi.org/10.5194/tc-2021-79, 2021.

Gelaro, R., McCarty, W., Suárez, M. J., Todling, R., Molod, A., Takacs, L., Randles, C. A., Darmenov, A., Bosilovich, M. G., Reichle, R., et al.: The modern-era retrospective analysis for research and applications, version 2 (MERRA-2), Journal of climate, 30, 5419–5454, 2017.

Gorshkov, S.: Atlas of Oceans: Arctic Ocean (in Russian). Mil, Def, 199, 1980.

Guerreiro, K. and Fleury, S.: LEGOS Altimetric Sea Ice Thickness Data Product v1., 2017.

Haas, C., Lobach, J., Hendricks, S., Rabenstein, L., and Pfaffling, A.: Helicopter-borne measurements of sea ice thickness, using a small and lightweight, digital EM system, Journal of Applied Geophysics, 67, 234–241, 2009.

Hendricks, S., Ricker, R., and Paul, S.: Product User Guide & Algorithm Specification: AWI CryoSat-2 Sea Ice Thickness (version 2.4), 2021.

Hersbach, H., Bell, B., Berrisford, P., Hirahara, S., Horányi, A., Muñoz Sabater, J., Nicolas, J., Peubey, C., Radu, R., Schepers, D., Simmons, A., Soci, C., Abdalla, S., Abellan, X., Balsamo, G., Bechtold, P., Biavati, G., Bidlot, J., Bonavita, M., De Chiara, G., Dahlgren, P., Dee, D., Diamantakis, M., Dragani, R., Flemming, J., Forbes, R., Fuentes, M., Geer, A., Haimberger, L., Healy, S., Hogan, R. J., Hólm, E., Janisková, M., Keeley, S., Laloyaux, P., Lopez, P., Lupu, C., Radnoti, G., de Rosnay, P., Rozum, I., Vamborg, F., Villaume, S., and Thépaut, J.-N.: Complete ERA5: Fifth generation of ECMWF atmospheric reanalyses of the global climate, Copernicus Climate Change Service (C3S) Data Store (CDS), accessed in 2021, 2017.

Hordoir, R., Skagseth, Ø., Ingvaldsen, R. B., Sandø, A. B., Löptien, U., Dietze, H., Gierisch, A. M., Assmann, K. M., Lundesgaard, Ø., and Lind, S.: Changes in Arctic Stratification and Mixed Layer Depth Cycle: A Modeling Analysis, Journal of Geophysical Research: Oceans, 127, e2021JC017 270, 2022.

https://doi.org/10.5194/tc-2023-122
Preprint. Discussion started: 14 August 2023

Hunke, E., Allard, R., Bailey, D. A., Blain, P., Craig, A., Dupont, F., DuVivier, A., Grumbine, R., Hebert, D., Holland, M., Jeffery, N., Lemieux, J.-F., Osinski, R., Rasmussen, T., Ribergaard, M., Roberts, A., Turner, M., Winton, M., and Rethmeier, S.: CICE Version 6.2.0, https://github.com/CICE-Consortium/CICE/tree/CICE6.2.0, 2021.

Janout, M. A., Hölemann, J., Laukert, G., Smirnov, A., Krumpen, T., Bauch, D., and Timokhov, L.: On the variability of stratification in the freshwater-influenced Laptev Sea Region, Frontiers in Marine Science, 7, 543 489, 2020.

Ji, Q., Li, B., Pang, X., Zhao, X., and Lei, R.: Arctic sea ice density observation and its impact on sea ice thickness retrieval from CryoSat–2, Cold Regions Science and Technology, 181, 103 177, 2021.

Jutila, A., Hendricks, S., Ricker, R., Albedyll, L. v., Krumpen, T., and Haas, C.: Retrieval and parametrisation of sea-ice bulk density from airborne multi-sensor measurements., Cryosphere Discussions, 2021.

Kern, S., Khvorostovsky, K., Skourup, H., Rinne, E., Parsakhoo, Z., Djepa, V., Wadhams, P., and Sandven, S.: The impact of snow depth, snow density and ice density on sea ice thickness retrieval from satellite radar altimetry: results from the ESA-CCI Sea Ice ECV Project Round Robin Exercise, The Cryosphere, 9, 37–52, 2015.

King, J., Skourup, H., Hvidegaard, S. M., Rösel, A., Gerland, S., Spreen, G., Polashenski, C., Helm, V., and Liston, G. E.: Comparison of freeboard retrieval and ice thickness calculation from ALS, ASIRAS, and CryoSat-2 in the Norwegian Arctic to field measurements made during the N-ICE2015 expedition, Journal of Geophysical Research: Oceans, 123, 1123–1141, 2018.

Kurtz, N., Farrell, S., Studinger, M., Galin, N., Harbeck, J., Lindsay, R., Onana, V., Panzer, B., and Sonntag, J.: Sea ice thickness, freeboard, and snow depth products from Operation IceBridge airborne data, The Cryosphere, 7, 1035–1056, 2013.

Kurtz, N. T. and Farrell, S. L.: Large-scale surveys of snow depth on Arctic sea ice from Operation IceBridge, Geophysical Research Letters, 38, 2011.

Kwok, R.: Simulated effects of a snow layer on retrieval of CryoSat-2 sea ice freeboard, Geophysical Research Letters, 41, 5014–5020, 2014.

Kwok, R., Panzer, B., Leuschen, C., Pang, S., Markus, T., Holt, B., and Gogineni, S.: Airborne surveys of snow depth over Arctic sea ice, Journal of Geophysical Research: Oceans, 116, 2011.

Kwok, R., Kacimi, S., Webster, M., Kurtz, N., and Petty, A.: Arctic snow depth and sea ice thickness from ICESat-2 and CryoSat-2 freeboards: A first examination, Journal of Geophysical Research: Oceans, 125, e2019JC016 008, 2020.

Landy, J. C., Dawson, G. J., Tsamados, M., Bushuk, M., Stroeve, J. C., Howell, S. E., Krumpen, T., Babb, D. G., Komarov, A. S., Heorton, H. D., et al.: A year-round satellite sea-ice thickness record from CryoSat-2, Nature, 609, 517–522, 2022.

Laxon, S., Peacock, N., and Smith, D.: High interannual variability of sea ice thickness in the Arctic region, Nature, 425, 947–950, 2003.

Liston, G. E., Itkin, P., Stroeve, J., Tschudi, M., Stewart, J. S., Pedersen, S. H., Reinking, A. K., and Elder, K.: A Lagrangian snow-evolution system for sea-ice applications (SnowModel-LG): Part I—Model description, Journal of Geophysical Research: Oceans, 125, e2019JC015 913, 2020.

MacGregor, J. A., Boisvert, L. N., Medley, B., Petty, A. A., Harbeck, J. P., Bell, R. E., Blair, J. B., Blanchard-Wrigglesworth, E., Buckley, E. M., Christoffersen, M. S., et al.: The scientific legacy of NASA's Operation IceBridge, 2021.

Madec, G., Bourdallé-Badie, R., Bouttier, P.-A., Bricaud, C., Bruciaferri, D., Calvert, D., Chanut, J., Clementi, E., Coward, A., Delrosso, D., et al.: NEMO ocean engine, 2017.

Mallett, R., Stroeve, J., Cornish, S., Crawford, A., Lukovich, J., Serreze, M., Barrett, A., Meier, W., Heorton, H., and Tsamados, M.: Record winter winds in 2020/21 drove exceptional Arctic sea ice transport, Communications Earth & Environment, 2, 1–6, 2021.

Oggier, M., Salganik, E., Whitmore, L., Fong, A. A., Hoppe, C. J. M., Rember, R., Høyland, K. V., Divine, D. V., Gradinger, R., Fons, S. W., Abrahamsson, K., Aguilar-Islas, A. M., Angelopoulos, M., Arndt, S., Balmonte, J. P., Bozzato, D., Bowman, J. S., Castellani, G.,

https://doi.org/10.5194/tc-2023-122
Preprint. Discussion started: 14 August 2023

Chamberlain, E., Creamean, J., D'Angelo, A., Damm, E., Dumitrascu, A., Eggers, S. L., Gardner, J., Grosfeld, L., Haapala, J., Immerz, A., Kolabutin, N., Lange, B. A., Lei, R., Marsay, C. M., Maus, S., Müller, O., Olsen, L. M., Nuibom, A., Ren, J., Rinke, A., Sheikin, I., Shimanchuk, E., Snoeijs-Leijonmalm, P., Spahic, S., Stefels, J., Torres-Valdés, S., Torstensson, A., Ulfsbo, A., Verdugo, J., Vortkamp, M., Wang, L., Webster, M., Wischnewski, L., and Granskog, M. A.: First-year sea-ice salinity, temperature, density, oxygen and hydrogen isotope composition from the main coring site (MCS-FYI) during MOSAiC legs 1 to 4 in 2019/2020, https://doi.pangaea.de/10.1594/PANGAEA.956732, 2023.

Pavlov, V. and Stanovoy, V.: Climate Signal in the Fluctuations of the Sea Level and River Run-Off in the Arctic Ocean, WORLD METEOROLOGICAL ORGANIZATION-PUBLICATIONS-WMO TD, pp. 184–186, 1998.

Pustogvar, A. and Kulyakhtin, A.: Sea ice density measurements. Methods and uncertainties, Cold Regions Science and Technology, 131, 46–52, https://doi.org/https://doi.org/10.1016/j.coldregions.2016.09.001, 2016.

Ricker, R., Hendricks, S., Helm, V., Skourup, H., and Davidson, M.: Sensitivity of CryoSat-2 Arctic sea-ice freeboard and thickness on radar-waveform interpretation, The Cryosphere, 8, 1607–1622, 2014.

SAF, O.: Global Sea Ice Type (netCDF) - Multimission, EUMETSAT SAF on Ocean and Sea Ice, https://doi.org/10.15770/EUM_SAF_OSI_NRT_2006, 2017.

Sallila, H., Farrell, S. L., McCurry, J., and Rinne, E.: Assessment of contemporary satellite sea ice thickness products for Arctic sea ice, The Cryosphere, 13, 1187–1213, 2019.

Shiklomanov, A., Déry, S., Tretiakov, M., Yang, D., Magritsky, D., Georgiadi, A., and Tang, W.: River freshwater flux to the Arctic Ocean, Arctic hydrology, permafrost and ecosystems, pp. 703–738, 2021.

Sievers, I., Rasmussen, T. A., and Stenseng, L.: Assimilating CryoSat-2 freeboard to improve Arctic sea ice thickness estimates, The Cryosphere Discussions, pp. 1–23, 2023.

Stroeve, J., Liston, G. E., Buzzard, S., Zhou, L., Mallett, R., Barrett, A., Tschudi, M., Tsamados, M., Itkin, P., and Stewart, J. S.: A Lagrangian snow evolution system for sea ice applications (SnowModel-LG): Part II—Analyses, Journal of Geophysical Research: Oceans, 125, e2019JC015 900, 2020.

Stroeve, J. C., Serreze, M. C., Barrett, A., and Kindig, D. N.: Attribution of recent changes in autumn cyclone associated precipitation in the Arctic, Tellus A: Dynamic Meteorology and Oceanography, 63, 653–663, 2011.

Tilling, R. L., Ridout, A., and Shepherd, A.: Estimating Arctic sea ice thickness and volume using CryoSat-2 radar altimeter data, Advances in Space Research, 62, 1203–1225, 2018.

Timco, G. and Frederking, R.: A review of sea ice density, Cold Regions Science and Technology, 24, 1–6, https://doi.org/https://doi.org/10.1016/0165-232X(95)00007-X, 1996.

Timokhov, L. and Tanis, F.: Environmental Working Group Joint US-Russian Atlas of the Arctic Ocean—Winter Period, Environmental Research Institute of Michigan in association with the National Snow and Ice Data Center, CD-ROM, 1997.

Tsamados, M., Feltham, D. L., Schroeder, D., Flocco, D., Farrell, S. L., Kurtz, N., Laxon, S. W., and Bacon, S.: Impact of variable atmospheric and oceanic form drag on simulations of Arctic sea ice, Journal of Physical Oceanography, 44, 1329–1353, 2014.

Wadhams, P., Tucker III, W., Krabill, W. B., Swift, R. N., Comiso, J. C., and Davis, N.: Relationship between sea ice freeboard and draft in the Arctic Basin, and implications for ice thickness monitoring, Journal of Geophysical Research: Oceans, 97, 20 325–20 334, 1992.

Wagner, D. N., Shupe, M. D., Cox, C., Persson, O. G., Uttal, T., Frey, M. M., Kirchgaessner, A., Schneebeli, M., Jaggi, M., Macfarlane, A. R., et al.: Snowfall and snow accumulation during the MOSAiC winter and spring seasons, The Cryosphere, 16, 2373–2402, 2022.

https://doi.org/10.5194/tc-2023-122
Preprint. Discussion started: 14 August 2023

Warren, S. G., Rigor, I. G., Untersteiner, N., Radionov, V. F., Bryazgin, N. N., Aleksandrov, Y. I., and Colony, R.: Snow depth on Arctic sea ice, Journal of Climate, 12, 1814–1829, 1999.

Willatt, R., Laxon, S., Giles, K., Cullen, R., Haas, C., and Helm, V.: Ku-band radar penetration into snow cover on Arctic sea ice using airborne data, Annals of Glaciology, 52, 197–205, 2011.

Wingham, D., Francis, C., Baker, S., Bouzinac, C., Brockley, D., Cullen, R., de Chateau-Thierry, P., Laxon, S., Mallow, U., Mavrocordatos, C., et al.: CryoSat: A mission to determine the fluctuations in Earth's land and marine ice fields, Advances in Space Research, 37, 841–871, 2006.

Zhou, L., Stroeve, J., Xu, S., Petty, A., Tilling, R., Winstrup, M., Rostosky, P., Lawrence, I. R., Liston, G. E., Ridout, A., et al.: Inter-comparison of snow depth over Arctic sea ice from reanalysis reconstructions and satellite retrieval, The Cryosphere, 15, 345–367, 2021.

Zweng, M., Seidov, D., Boyer, T., Locarnini, M., Garcia, H., Mishonov, A., Baranova, O., Weathers, K., Paver, C., Smolyar, I., et al.: World ocean atlas 2018, volume 2: Salinity, 2019.

Zweng, M. M., Boyer, T. P., Baranova, O. K., Reagan, J. R., Seidov, D., and Smolyar, I. V.: An inventory of Arctic Ocean data in the World Ocean Database, Earth System Science Data, 10, 677–687, https://doi.org/10.5194/essd-10-677-2018, 2018.

Zygmuntowska, M., Rampal, P., Ivanova, N., and Smedsrud, L. H.: Uncertainties in Arctic sea ice thickness and volume: new estimates and implications for trends, The Cryosphere, 8, 705–720, https://doi.org/10.5194/tc-8-705-2014, 2014.